Phenol-benzene complexation dynamics: Quantum chemistry calculation, molecular dynamics simulations, and two dimensional IR spectroscopy

Kijeong Kwac,[a] Chewook Lee, Yousung Jung,[b] and Jaebeom Han
Department of Chemistry, Korea University, Seoul 136-701, Korea and Center for Multidimensional Spectroscopy, Korea University, Seoul 136-701, Korea

Kyungwon Kwak, Junrong Zheng, and M. D. Fayer
Department of Chemistry, Stanford University, Stanford, California 94305

Minhaeng Cho
Department of Chemistry, Korea University, Seoul 136-701, Korea and Center for Multidimensional Spectroscopy, Korea University, Seoul 136-701, Korea

(Received 6 September 2006; accepted 8 November 2006; published online 28 December 2006)

Molecular dynamics (MD) simulations and quantum mechanical electronic structure calculations are used to investigate the nature and dynamics of the phenol-benzene complex in the mixed solvent, benzene/CCl_4. Under thermal equilibrium conditions, the complexes are continuously dissociating and forming. The MD simulations are used to calculate the experimental observables related to the phenol hydroxyl stretching mode, i.e., the two dimensional infrared vibrational echo spectrum as a function of time, which directly displays the formation and dissociation of the complex through the growth of off-diagonal peaks, and the linear absorption spectrum, which displays two hydroxyl stretch peaks, one for the complex and one for the free phenol. The results of the simulations are compared to previously reported experimental data and are found to be in quite reasonable agreement. The electronic structure calculations show that the complex is T shaped. The classical potential used for the phenol-benzene interaction in the MD simulations is in good accord with the highest level of the electronic structure calculations. A variety of other features is extracted from the simulations including the relationship between the structure and the projection of the electric field on the hydroxyl group. The fluctuating electric field is used to determine the hydroxyl stretch frequency-frequency correlation function (FFCF). The simulations are also used to examine the number distribution of benzene and CCl_4 molecules in the first solvent shell around the phenol. It is found that the distribution is not that of the solvent mole fraction of benzene. There are substantial probabilities of finding a phenol in either a pure benzene environment or a pure CCl_4 environment. A conjecture is made that relates the FFCF to the local number of benzene molecules in phenol's first solvent shell. © *2006 American Institute of Physics*. [DOI: 10.1063/1.2403132]

I. INTRODUCTION

The nature of organic solutes in liquid solutions is a fundamentally interesting problem that is also of practical importance in chemistry, biology, and materials science. In the simplest view, the solute can be taken to be in a homogenous dielectric continuum.[1] However, a more realistic approach is to consider the radial distribution function of the solvent about a solute.[2] The radial distribution function brings in solvent shells and can account for the influence of solvent structure on the relative positions of solutes[2,3] and diffusion through the structured solvent by including a potential of mean force in a description of transport.[2,3] However, organic solutes and solvents have anisotropic intermolecular interactions. Such interactions may not be negligible compared to thermal energy, k_BT, at room temperature. Therefore, transitory organic solute-solvent complexes can form and exist for times that depend on the strength of the solute-solvent intermolecular interactions. Such complexes have the potential to influence chemical reaction kinetics by blocking reaction sites on a solute. In effect, the solute-solvent dissociation reaction may have to take place before another chemical reaction with the solute can occur.

Recently, the first direct measurements of organic solute-solvent complex formation and dissociation under thermal equilibrium conditions were made using ultrafast infrared vibrational echo chemical exchange experiments.[4–6] Ultrafast IR methods have been used extensively to study the dynamics of extended hydrogen bonding systems such as water,[7–22] alcohols,[23–32] and nanoscopic water.[33–41] The "complexes" in water and alcohols are extended structures with a very wide variety of geometries and strengths of association. The organic solute-solvent complexes that will be discussed here involve a molecular pair with more or less a single structure and bond strength. Similar to the complexes discussed below is a hydrogen bonded pair of molecules in a solvent. Such a system has been studied using both two color pump-probe spectroscopy[42] and two-dimensional (2D) vibrational chemi-

[a]Present address: Department of Chemistry, University of California at San Diego, La Jolla, CA 92093.
[b]Present address: Department of Chemistry, California Institute of Technology, Pasadena, CA 91125.

cal exchange spectroscopy,[43] the experimental method used to obtain the solute-solvent complex data discussed here.

A number of different organic solute-solvent complexes have been studied using 2D vibrational echo chemical exchange experiments to determine the dynamics of complex formation and dissociation.[4,5] The system that is the simplest chemically is the phenol-benzene complex. In the solution, phenol is the low concentration solute in a mixed solvent of benzene and CCl_4. CCl_4 is added to the benzene solvent to shift the equilibrium toward more uncomplexed (free) phenol. In pure benzene, the fraction of phenol that is complexed is >90%, which makes the system difficult to study experimentally. In the mixed solvent employed in the experiments, there is approximately a 50-50 mixture of phenol complex and free phenol.[4] The two species have distinct Fourier transform infrared (FTIR) spectra of the hydroxyl stretch. In the experiments, the hydroxyl H is replaced with D, and the OD hydroxyl stretch frequency of free phenol in the mixed solvent is at 2665 cm^{-1} and the frequency of the complex is at 2631 cm^{-1}. Figure 1(a) shows the FTIR spectrum. Although the spectra of the two species overlap, the two peaks are readily observable.[4] FTIR experiments were used to determine the equilibrium constant and the complex formation enthalpy and entropy.[4] However, the linear absorption experiments cannot provide information on the time dependence of the complex formation and dissociation.

In a 2D IR vibrational echo experiment, three ultrashort IR pulses are tuned to the frequency of the vibrational modes of interest and crossed in the sample. Because the pulses are very short, the hydroxyl stretch of both the complex and free phenol are simultaneously excited. The times between pulses 1 and 2 and pulses 2 and 3 are called τ and T_w, respectively. At a time $\leqslant\tau$ after the third pulse, a fourth IR pulse is emitted in a unique direction. This is the vibrational echo, the signal in the experiments. The vibrational echo is the infrared vibrational equivalent of the magnetic resonance spin echo[44] and the electronic excitation photon echo.[45] The vibrational echo is combined with another pulse, the local oscillator, and heterodyne detected. Therefore, both amplitude and phase information are obtained. The combined vibrational echo-local oscillator is passed through a monochromator and frequency resolved. The spectrum is an experimental Fourier transform, which provides one of the two Fourier transforms that gives rise to the 2D vibrational echo spectrum. When τ is scanned, an interferogram is produced between the vibrational echo and the local oscillator. One such interferogram is generated at each frequency at which there is vibrational echo emission. The numerical Fourier transforms of these interferograms provide the second Fourier transform for the 2D spectrum. Details of the experimental method used for these experiments have been given previously.[21]

In a dynamic system, the first laser pulse "labels" the initial structures of the species in the sample. The second pulse ends the first time period τ and starts clocking the "reaction time," during which the "labeled" species experience population dynamics. The third pulse ends the population dynamics period of length T_w, and begins a third period of length $\leqslant\tau$, which ends with the emission of the vibrational echo pulse. The echo signal reads out the information

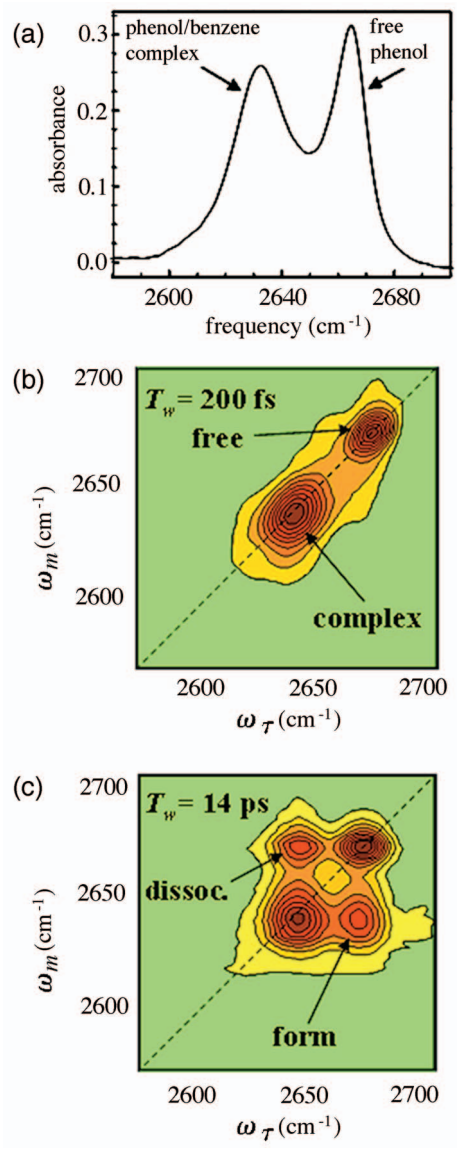

FIG. 1. (Color) (a) FTIR spectra of the OD hydroxyl stretch of phenol for the phenol-benzene complex and free phenol in the benzene/CCl_4 mixed solvent. (b) 2D vibrational echo spectrum at a time (200 fs) short compared to complex formation and dissociation showing two peaks on the diagonal. (c) 2D vibrational echo spectrum at a time (14 ps) long compared to complex formation and dissociation showing two peaks on the diagonal and two addition off-diagonal peaks. The off-diagonal peaks grow in as complex formation and dissociation proceed.

about the final structures of all labeled species. In the chemical exchange problem under consideration here, the two species, complexed and free phenol, are in equilibrium. They are interconverting one to the other without changing the overall number of either species. In an experiment, τ is scanned for fixed T_w. The recorded signals are converted into a 2D vibrational echo spectrum. Then T_w is increased and another spectrum is obtained. Chemical exchange between the complex and free species causes new off-diagonal peaks to grow in as T_w is increased. Figure 1(b) displays a 2D vibrational echo spectrum taken at T_w=200 fs, which is a time short compare to the chemical exchange time. The spectrum shows two peaks on the diagonal (dashed line), one is the spectrum of the free phenol, and the other is the complex. Figure 1(c)

displays the data at $T_w = 14$ ps, which is a time that is relatively long compared to the chemical exchange time. Now, in addition to the two diagonal peaks, two off-diagonal peaks have grown in, one caused by dissociation of complexes and the other by the formation of complexes from free phenol. When combined with other parameters of the system that are independently measured, the growth of the off-diagonal peaks as T_w is increased from short to long time permits the complex dissociation and formation kinetics to be directly determined.[4,6] Because the complex and free phenol are in equilibrium, the number of complexes per unit time dissociating is equal to the number of complexes forming. Therefore, the process can be characterized by the single parameter, the complex dissociation time, τ_d, which is the inverse of the complex dissociation rate. It was found from the 2D vibrational echo experiments that the phenol-benzene dissociation time, $\tau_d = 8$ ps.[4]

Although the 2D experiments measured the dissociation time for the phenol-benzene complex, the experiments do not give a microscopic picture of the nature of the process. Ultrafast IR experiments on water[7–22] have been greatly augmented by applying molecular dynamics (MD) simulations and other theoretical calculations to understand the implications of the experimental results.[13,14,17–20,46–58] For water, the MD simulations address the dynamic structure of the extended hydrogen bond network and relate the calculations to the experimental observables. Recent applications of MD simulations to the theoretical calculations of one dimensional (1D) and 2D spectra of *N*-methylacetamide in water showed that the simulation method can provide detailed information on the hydrogen bond making and breaking dynamics of water and methanol molecules in the first solvation shell of *N*-methylacetamide.[59–62] Here, we will take a similar path for understanding the structure and dynamics of organic solute-solvent complexes. There are a variety of issues to be clarified, which can only be done by theoretical studies. These issues include the existence of stable phenol-benzene complexes, the conformation of the complexes, the dispersive interaction strength, the intermolecular potential energy surface, the set of classical force field (FF) parameters closely mimicking the quantum potential surface, local solvation structures and dynamics, and so on.

In this paper, we will present detailed theoretical descriptions of phenol-benzene complex formation and energetics and the importance of dispersive interaction, using HF, DFT, and MP2 calculation methods. Comparing these different calculation results, a reliable potential energy surface is obtained that is necessary to properly develop the classical FF parameters for MD simulations. Then, using the optimized FF parameters, MD simulations of phenolOD in benzene/CCl_4, phenolOD in benzene, and phenolOD in CCl_4 solutions are carried out. In order to quantitatively simulate the 1D and 2D vibrational spectra, the electric field (Stark effect) model is employed. In this model, the time dependent OD frequency is linearly proportional to the electric field projected along the direction of the hydroxyl bond at the center of the OD group. The resulting calculated IR absorption and 2D vibrational echo spectra are directly compared with experimental results.[4,6] Also, the local inhomogeneous environment around the OD chromophore and domain formations in phenolOD in benzene/CCl_4 solvent are discussed in detail.

II. QUANTUM CHEMISTRY CALCULATIONS

In this section, we present the results of a variety of quantum chemistry calculations for the complexation of phenol with benzene. Accurate binding energies and harmonic vibrational frequencies of the complex, particularly of the OD stretch mode of phenolOD under different molecular environments, are the main focus of this section.

Long-range electron correlation effects, such as dispersion interactions, are important in describing weakly interacting van der Waals (vdW) systems such as the one under consideration here, but their theoretical treatment is by no means trivial. For example, such effects are absent in Hartree-Fock (HF) or current Kohn-Sham density functional theory (DFT) implementation,[63] which is the most popular electronic structure method used today. One of the extensively studied examples is the benzene dimer, which is predicted to be unstable by HF and almost all standard DFT functionals.[64,65] In spite of the fact that HF and DFT can describe electrostatics fairly well, it has been shown that some vdW complexes are calculated by HF and DFT not to be bound.[63,66,67] However, stable bound complexes are theoretically reproduced only at theoretical levels that include correlation. The differing results obtained with HF and DFT versus theories with correlation are often used to indicate the importance of dispersion interactions in such vdW systems.[64,65]

This limitation of HF and DFT in taking into account the long-range correlation effects has been, in large part, remedied by Møllet-Plesset theory (MP2).[68] MP2 is the simplest wave-function-based method that can correctly describe the long-range correlation effects, although it generally overshoots the binding energies by overestimating such effects. Coupled-cluster with single and double and perturbative triple [CCSD(T)] excitations,[69] on the other hand, *if computationally tractable* for a given system, is probably the most accurate *ab initio* method that is currently available to treat nonbonded vdW systems.

Another computationally useful and relatively less time consuming alternative is the recently proposed scaled opposite spin (SOS) MP2 scheme, in which the opposite spin (OS) correlation energy is scaled up by an empirical factor, c_{OS}, while entirely neglecting the same spin counterpart.[70] Associated computational savings is the reduction of computational scaling by one power, from the fifth to the fourth order, while yielding statistically improved quantitative results over conventional MP2. More recently, SOS-MP2 with $c_{OS} = 1.55$, denoted as SOS-MP2 (1.55), was proposed to specifically study vdW complexes with an aim to reproducing CCSD(T) binding energies with substantially less computational effort.[76] Hence, in this study, in addition to well-known HF and DFT methods we also used MP2, SOS-MP2 (1.55), and CCSD(T) to assess the differences in the results produced by these methods and to obtain accurate binding

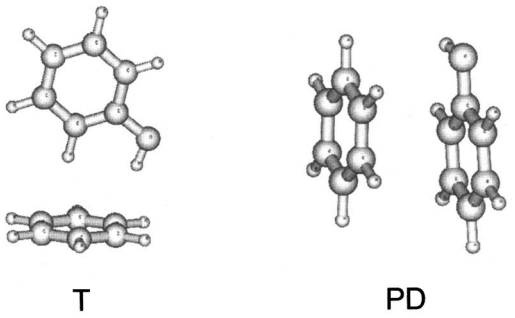

FIG. 2. RI-MP2 optimized T-shaped (T) and parallel-displaced (PD) structures of the phenol-benzene complex. Interplanar distance between benzene and phenol rings in the PD complex is 3.14 Å.

energies of the phenol-benzene complex. Efficient resolution of the identity implementation of MP2, namely, RI-MP2,[71] was used for MP2.

All interaction (or complexation) energies reported in this paper were counterpoise corrected for basis set superposition error (BSSE),[72] which usually makes the vdW complex binds too strongly. BSSE is the borrowing of basis functions from the second monomer to improve the quality of basis functions of the first monomer relative to the same monomer in isolation and can occur for any chemical interaction between the fragments that employ finite basis sets. We used two sets of basis functions, 6-311++G(d,p) and aug-cc-pVXZ (X=D,T,Q), that include diffuse functions that are important for a good long-range description of weakly interacting nonbonded systems. In particular, the augmented correlation consistent basis sets of Dunning (aug-cc-pVXZ, where X=D,T,Q) were chosen because they can be systematically extrapolated to the complete basis set (CBS) limit using the following two-point extrapolation prescription for correlation energies.[73] In this study, we used DT extrapolation.

$$E_{\mathrm{CBS}}[XY] = E_Y^{\mathrm{SCF}} + \frac{X^3 E_X^{\mathrm{Corr}} - Y^3 E_Y^{\mathrm{Corr}}}{X^3 - Y^3}, \quad Y > X. \tag{1}$$

HF and B3LYP density functional theory calculations were performed using GAUSSIAN03,[74] while all the other correlation calculations, RI-MP2, CCSD(T), and SOS-MP2, were carried out using the Q-CHEM3.0 *ab initio* program package.[75]

Two stable configurations were found for the phenol-benzene system, namely, T-shaped (T) and parallel-displaced (PD) structures, which are depicted in Fig. 2. These structures are reminiscent of the benzene dimer, and for that reason we will emphasize some similarities and differences between them when appropriate. The principal results are summarized in Table I. The T-shaped phenol-benzene complex is stable even at the HF and B3LYP levels by −1.90 and −2.0 kcal/mol, respectively, unlike that of benzene dimer.[76] The stability manifested in these calculations suggests relatively strong electrostatic attraction between benzene and phenol, which has a permanent dipole moment. The phenol-benzene dipole-quadrupole interaction is stronger than the interaction between two quadrupole moments of benzene in T-shaped benzene dimer. The strength of the phenol-benzene electrostatic interactions outweighs the exchange repulsion, resulting in the net binding even without considering dispersion effects. By contrast, the PD configuration, where the dispersion interactions are expected to be the more important source of attraction due to its cofacial geometry but which also causes more repulsion, is not bound at the HF and B3LYP levels, because these methods lack of long-range correlation effects.

TABLE I. Counterpoise corrected interaction energies (kcal/mol) for the T-shaped (T) and parallel-displaced (PD) configurations of phenol-benzene complex (see also Figs. 1 and 2).

Method	Basis	T	PD
HF	6-311++G**	−1.90	[a]
B3LYP	6-311++G**	−2.00	[a]
RI-MP2[b]	CBS[c]	−6.57	−6.28
CCSD(T)[d]	CBS	−5.46	−3.38
SOS-MP2 (1.55)[b,e]	CBS[c]	−5.05	−3.48

[a]PD configuration is unstable at the HF and B3LYP level.
[b]Alhrichs's corresponding auxiliary basis sets, that were designed be used in conjunction with aug-cc-pVXZ regular basis, were used.
[c]Extrapolated to the complete basis set (CBS) limit using Dunning's aug-cc-pV(DT)Z two-point extrapolation scheme for correlation energies.
[d]ΔE(CCSD(T)/CBS)=ΔE(RI-MP2/CBS)+[ΔE(CCSD(T)/6-31G*) −ΔE(RI-MP2/6-31G*)].
[e]SOS-MP2/aug-cc-pV(DT)Z with one parameter c_{OS}=1.55, which was proposed for a target accuracy of CCSD(T)/CBS (Ref. 76).

Upon incorporating the long-range correlations via MP2, CCSD(T), and SOS-MP2, the PD complex is found to be bound, and also the binding energy of T-shaped configuration becomes even larger at these levels than those obtained by using the HF or DFT methods (Table I). MP2 yields the highest values for the binding energies of the complexes, which are expected to be overestimated, while CCSD(T) yields smaller values. Specifically, at the CCSD(T)/CBS limit, the T-shaped complex is found to be the lowest energy configuration with the association energy of −5.46 kcal/mol, while the PD configuration is predicted to be another stable form with an interaction energy of −3.38 kcal/mol. It is also quite encouraging that the one-parameter SOS-MP2 (1.55) proposed earlier reproduces the CCSD(T)/CBS binding energies very well, with the stability of T configuration slightly underestimated as predicted previously.[76]

The potential energy curves for the T-shaped configuration as a function of phenol-benzene ring center-to-ring center distances are shown in Fig. 3, which graphically illustrates how each method performs relative to CCSD(T)/CBS. Again, the MP2 well depth is too deep, but the SOS-MP2 (1.55) curve overlaps remarkably well with that of CCSD(T)/CBS.

Next, we calculated harmonic vibration frequencies for the optimized T and PD configurations. In particular, the change of hydroxyl stretch mode of phenol for different molecular environments (i.e., free versus complex forms) can serve as a good spectroscopic signature that identifies the structure of the complex when combined with proper calculations. We therefore computed the OD stretch frequencies of phenolOD for the free and benzene-bound forms (T and PD) of phenol, and compared them with the experimental frequencies. The estimated shifts in OD stretch frequency when

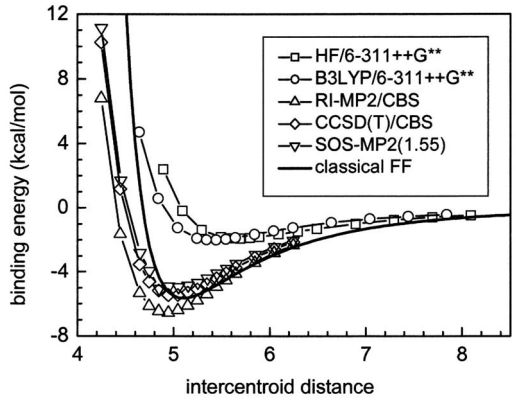

FIG. 3. Potential energy curves for the T-shaped configuration of phenol-benzene complex as a function of a ring-center to ring-center distance between them.

going from the free to complex forms are summarized in Table II. The OD bond strength becomes weaker in accord with the shift of 34 cm^{-1} to lower frequency upon complexation with benzene [see Fig. 1(a)]. Similar trends of weakened OD bond strengths in the complex forms are observed in HF, B3LYP, and MP2 calculations. The frequency shift for the T configuration (49 cm^{-1}) obtained with MP2 (which was the only level of theory among HF, B3LYP, and MP2 employed in this study that also predicted the PD complex to have a minimum) agrees better with experiments (34 cm^{-1}) than that for PD (11 cm^{-1}). Therefore, this fact together with the energetic consideration that the T-shaped complex is the lowest energy minimum by a significant amount suggests that the experimentally observed single complex species is most likely the T-shaped configuration.

The results of the high level electronic structure calculations also demonstrate the importance of the solvent on the energetics of the complex. The structure calculations are for a pair of molecules in the absence of the solvent. The complex enthalpy of formation in the mixed benzene/CCl_4 solvent was determined experimentally to be −1.67 kcal/mol.[4] In contrast, the best electronic structure methods yield approximately −5 kcal/mol (see Table I). In the electronic structure calculations, there is no competition between the phenol-benzene interaction and the interaction of the molecules that make up the complex with solvent molecules. For example, the solvation free energies of benzene and phenol in CCl_4 were recently estimated to be −4.2 and −6.6 kcal/mol, respectively.[77] Assuming that both solutes disturb the solvent structure to a similar and only minor extent so that the solvation free energies are dominated by the enthalpy contributions, both solutes have relatively strong interactions with CCl_4.

III. THE FORCE FIELD PARAMETERS AND MD SIMULATION METHOD

A. Force field parameters for benzene and phenol

The force field parameters of benzene and phenol molecules are determined using the Antechamber module of AMBER8 molecular dynamics package.[78] We have optimized the structures of benzene and phenol using the GAUSSIAN98 program with the HF/6−31G* basis set. The optimized structures are used as input to the Antechamber program to obtain the partial charges and geometrical parameters for MD simulations. The partial charge parameter for benzene is determined as $q_D=-q_C=0.1299e$. We denote the carbon atom attached to OD in the phenol molecule as C and denote the other carbon atoms as C1, C2, C3 in the order of distance from C, $q_O=-0.5569e$, $q_D=0.3781e$, $q_C=0.4279e$, $q_{C1}=-0.3236e$, $q_{H1}=0.1777e$, $q_{C2}=-0.0931e$, $q_{H2}=0.1439e$, $q_{C3}=-0.1996e$, and $q_{H3}=0.1408e$, where D is bonded to O and H1 is bonded to C1, etc. Only the charge parameters of four out of the six carbons are necessary due to the symmetry of the phenol molecule. We have implemented an equilibration run of the system consisting of a single phenol molecule and 384 benzene molecules under constant temperature and pressure conditions at 298 K and 1 bar for 800 ps. It takes ~200 ps to reach a plateau value of the density. The average value of the density for the last 500 ps trajectory is 0.873 g/cm^3, which is close to the experimental value of 0.879 g/cm^3 for pure benzene.

For the FF parameters of CCl_4, we used the OPLS-AA model.[79] The adopted parameters are r(C−Cl)=1.769 Å, $\sigma_C=3.80$ Å, $\sigma_{Cl}=3.47$ Å, $\varepsilon_C=0.050$ kcal/mol, $\varepsilon_{Cl}=0.266$ kcal/mol, and $q_C=-4q_{Cl}=0.248e$. We implemented an equilibration run of the system consisting of a single phenol molecule and 645 CCl_4 molecules under constant temperature and pressure conditions at 298 K and 1 bar for 800 ps. It

TABLE II. Characteristic OD stretch vibration frequencies (cm^{-1}) of phenol, with and without complexation with benzene. The T-shaped (T) and parallel-displaced (PD) complex configurations were considered. The PD configuration is found unstable at the HF and B3LYP level (see also Table I)

		Complex		Difference	
Method	Free	T	PD	Δ^a (T)	Δ^a (PD)
HF/6-311++G**[b]	2762	2743	⋯	19	⋯
B3LYP/6-311++G**[c]	2686	2641	⋯	45	⋯
MP2/6-311++G**[d]	2680	2631	2669	49	11
Expt.	2665	2631		34	

[a]Δ(T,PD)=ν(free)-ν (complex: T, PD).
[b]Frequency scaling factor=0.9051 was used (Ref. 88).
[c]Frequency scaling factor=0.9614 was used (Ref. 88).
[d]Frequency scaling factor=0.9500 was used (Ref. 88).

TABLE III. Distances between the centers of the rings and the binding energies for the T-shaped configuration of benzene-phenol complex.

Calculation level	Basis set (No. of basis functions)	Shape	Intercentroid distance (Å)	Binding energy (kcal/mol)
HF	6-311G(*d*) (270)	T	5.607	2.22
	6-311++G(*d*,*p*) (370)	Twisted T	5.694	1.90
	cc-pVDZ (242)	T	5.665	2.03
	aug-cc-pVDZ	T	5.645	1.40
B3LYP	6-311G(*d*) (270)	Tilted T	5.393	2.32
	6-311G(*d*) (270)	T	5.356	2.46
	D95 (154)	Twisted T	5.438	2.65
	D95++** (332)	T	5.343	2.23
	6-311++G(3*df*,2*pd*) (687)	T	5.413	1.92
	cc-pVDZ (242)	T	5.370	2.09
	aug-cc-pVTZ (874)	T	5.645	1.23
B3PW91	6-311G(*d*) (270)	Tilted and Twisted T	5.381	1.94
RI-MP2	aug-cc-pVDZ (407)	T	5.045	5.64
	aug-cc-pVTZ (874)	T	4.945	6.25
	CBS	T	4.945	6.56
Classical FF		T	5.099	5.65

takes about 50 ps to reach a plateau value of the density for this system. The average density of the last 500 ps is 1.581 g/cm^3, which is close to the experimental value of 1.594 g/cm^3 for pure CCl_4.

B. MD simulation method

We have done the MD simulations of three systems: phenol in benzene, phenol in CCl_4, and phenol in the mixed solvent benzene/CCl_4. The numbers of molecules used in the phenol in benzene and phenol in CCl_4 systems are mentioned in the previous section. To simulate the molecular dynamics of a phenol molecule in the mixture of benzene and CCl_4, we use a single phenol molecule and 192 benzene molecules and 480 CCl_4 molecules. The mole fraction of benzene is 0.286, which is very close to the experimental conditions.

The Sander module of the AMBER 8 program package[78] was used for the simulations. Each system is placed in a cubic box with a periodic boundary condition. Long range electrostatic interactions are treated by the particle mesh ewald[80] (PME) method and the criterion to switch from direct sum to the calculation by PME is 9 Å. The initial system is minimized by 500 steps of steepest-descent minimization and 500 steps of conjugate-gradient method minimization with the solute molecule fixed. Then, the total system is minimized by 1500 steps of the steepest-descent method and 1000 steps of the conjugate gradient method. The system is equilibrated under the constant temperature and pressure conditions of 298 K and 1 bar for 800 ps and then under constant temperature conditions for 200 ps. After that, a 4 ns production run is implemented under the constant temperature condition of 298 K. All the constant temperature and pressure conditions are implemented using the weak coupling algorithm of Berendsen *et al.*[81] The time step for the equilibration and production runs is 1 fs.

C. Comparisons of the classical force field with the quantum chemistry calculations

As a test for the classical FF parameters, we calculated the interaction energy of the T-shaped phenol-benzene complex as a function of the distance between the ring centers of the two molecules. The result is plotted in Fig. 3 along with the quantum chemistry calculation results (see the solid curve). Also we show the location of the potential minimum and the binding energy as the minimum value of the potential energy curve in Table III.

One of the notable features is that the classical FF (in Fig. 3) produces the potential energy curve which is close to the quantum chemistry methods that correctly describe long-range correlation effects [RI-MP2, CCSD(T), and SOS-MP2 in Fig. 3]. While the classical potential has the steeper repulsive part at short distance, the overall shape and the magnitude of binding energy are well matched to the results of the SOS-MP2 and CCSD(T) method. In the configuration corresponding to the potential minimum under the classical FF, the distance between the ring center of benzene and the D-atom of phenol OD group is 2.39 Å.

We calculated the pair distribution between the ring center of benzene and the D atom of phenol OD group from snapshot structures found in the MD simulation. The result for the phenol in benzene/CCl_4 system is shown in Fig. 4. The first maximum is located at 2.55 Å. This value is larger than the value of 2.39 Å for the minimum energy configuration for the phenol-benzene without solvent. As in the comparison of the calculated complex energy and the experimentally determined entropy[4] (see discussion at the very end of Sec. II), the increase in separation demonstrates the influence of the solvent on the complex structure. To make this argument quantitative, using the theorem, $g(r)=\exp(-w(r)/k_BT)$, where $w(r)$ is the potential of mean force (PMF), we calcu-

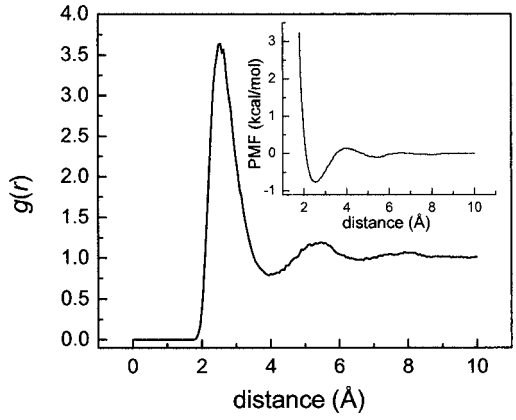

FIG. 4. The pair distribution function for the distance between the center of mass of benzene and the D atom of phenol OD group. The potential of mean force obtained using $g(r)=\exp(-w(r)/k_BT)$ is plotted in the inset.

lated $w(r)$ (see the inset of Fig. 4). The estimated binding energy from PMF is about −0.78 kcal/mol. This is about half of the experimentally measured complex enthalpy of formation, −1.67 kcal/mol.[4]

From the MD trajectories, we analyzed the configuration of the phenol-benzene complex in detail. We picked the benzene molecule which is nearest to the phenol molecule at each snapshot configuration in the MD trajectory for the phenolOD in benzene/CCl_4 system. We denote the angle between the two vectors that are normal to the benzene and phenol ring planes as θ, and the distance between the ring center of benzene and the D atom of phenol OD group as R. We plot the population of phenol-benzene geometry with respect to θ and R in Fig. 5. It should be noted that the distribution of θ is broad, indicating the potential energy surface along this angle for a fixed intermolecular distance R is shallow. However, it is clear that the preferred geometry is T shaped as was argued in Sec. II based on electronic structure calculations. The configurations with the $R>4$ Å correspond to the situation where phenol is solvated by the CCl_4 molecules, that is, there is no complex.

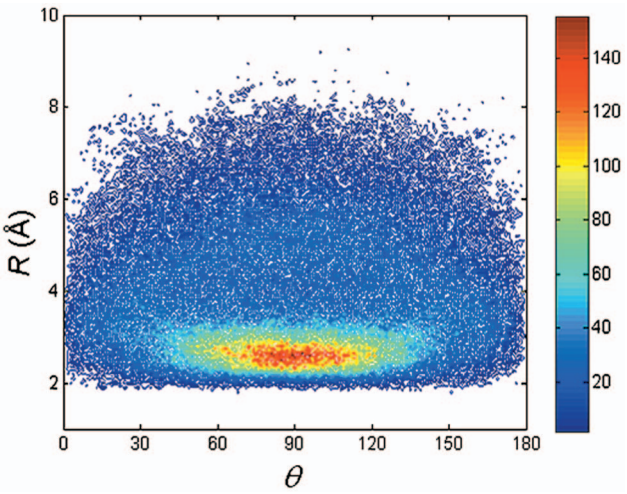

FIG. 5. (Color) Population for the configuration of the benzene molecule nearest to the phenol molecule at each MD snapshot with respect to R and θ, where R denotes the distance between the ring center of benzene and D atom of the OD group of phenol and θ denotes the angle between the normal vectors at the two ring centers of benzene and phenol.

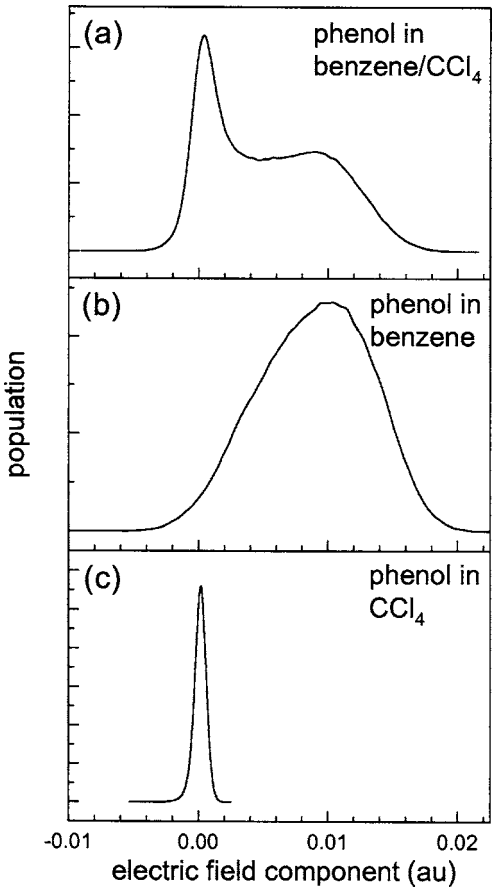

FIG. 6. Distribution of the projection, E, of the electric field in a.u. along the OD bond evaluated at the site of the D atom of the phenol molecule.

IV. VIBRATIONAL SPECTRA: COMPARISON BETWEEN MD SIMULATIONS AND EXPERIMENT

A. OD stretching mode frequency from MD trajectories

To numerically simulate the 1D and 2D IR spectra, it is necessary to obtain the fluctuating transition frequency trajectory from the MD simulations. Here, we will use the vibrational Stark effect theory, where the OD stretching mode frequency is assumed to be linearly proportional to the electric field, E, as[82]

$$\omega_{\mathrm{OD}}(t) = \omega_{\mathrm{OD}}^0 + \kappa E(t), \tag{2}$$

where E is the component of the electric field along the OD bond evaluated at the position of the D atom, i.e.,

$$E(t) = \hat{r}_{\mathrm{OD}}(t) \sum_{m,i} \frac{q_{mi}}{r_{mi,\mathrm{D}}^2(t)} \hat{r}_{mi,\mathrm{D}}(t). \tag{3}$$

The unit vector along the OD bond is denoted as $\hat{r}_{\mathrm{OD}}$. q_{mi} and $r_{mi,\mathrm{D}}$ ($\hat{r}_{mi,\mathrm{D}}$) are the partial charge of the ith atom of the mth solvent molecule and the magnitude (unit vector) of the distance vector pointing from the ith atom of the mth solvent molecule to the D atom of the phenol.

From the three separated MD simulations, phenol in the mixed solvent, in pure benzene, and in pure CCl_4, the electric field component distributions were calculated. The results are plotted in Fig. 6 (E is in a.u.). As can be seen in Fig. 6(c), when phenol is dissolved in pure CCl_4, the projected

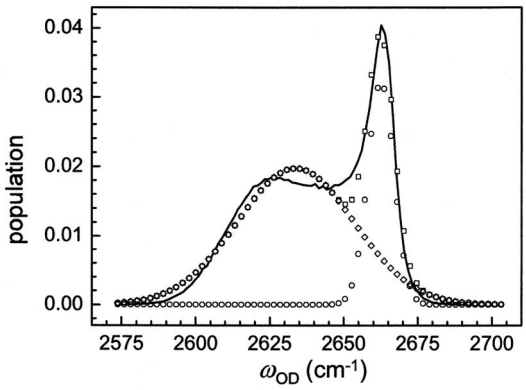

FIG. 7. Population distribution of OD stretch mode frequency. Two fitted Gaussian functions are also plotted (open circles and squares). Total fitting results are plotted as closed squares.

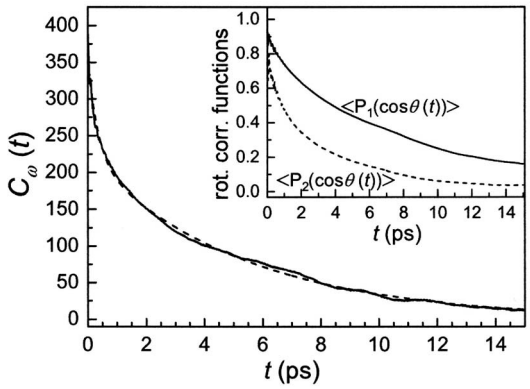

FIG. 8. OD stretch mode frequency-frequency correlation function. The dashed curve is a biexponential fit. The two rotational correlation functions $C_1(t)$ and $C_2(t)$ obtained from MD trajectories are plotted in the inset.

electric field along the phenol OD group at the position of the D is centered virtually at zero, indicating that the solvatochromic OD frequency shift induced by the phenol-CCl_4 interaction is exceedingly small. However, it should be mentioned that the OD stretch frequency of phenol in CCl_4 would be different from the gas phase phenol OD stretch frequency, indicating that the OD frequency shift can be induced by solute-solvent interaction other than the electric field effect. This, however, is beyond the scope of this work and should be a subject of future investigation. Nevertheless, the electrostatic intermolecular interaction between phenol and benzene can greatly affect the OD frequency and induces a strong redshift. The influence of benzene on the electric field distribution is clearly seen in Figs. 6(a) and 6(b). In Fig. 6(b), phenol in pure benzene, there is a broad electric field distribution shifted to high field. The IR absorption spectrum of phenol in pure benzene shows that phenol exists almost completely as the phenol benzene complex, with very little free phenol.[4,6] In the mixed solvent [Fig. 6(a)], there are two peaks that clearly correspond to the peaks in Figs. 6(b) and 6(c).

The two constants, ω_{OD}^0 and κ, in Eq. (2) are obtained by noting that the high- and low frequency bands in the experimentally measured IR absorption spectrum[4] [see Fig. 1(a)] correspond to the free phenol and the phenol-benzene complex, respectively. The free phenol peak in the mixed solvent is very similar to the IR absorption spectrum of phenol in pure CCl_4,[4] while the complexed peak is very similar to the spectrum of phenol in pure benzene. The constant $\omega_{OD}^0 = 2665\ \text{cm}^{-1}$ was assigned to the high frequency band, and $\kappa = -4229$ was determined from the frequency difference between the two bands. Using these constants and Eq. (2), the time-dependent frequency $\omega_{OD}(t)$ can be calculated from the MD trajectories. Figure 7 shows the population of frequencies, which is just the probability of having a frequency per unit time obtained from $\omega_{OD}(t)$. The frequency-dependent population cannot be compared directly to the spectrum in Fig. 1(a) not only because the transition dipoles are different for free phenol and the complex but also because the line broadening process is not taken into account.[4] However, it has qualitatively similar features. The peak positions are close to the experimental values and the redshifted peak is broader than the peak to the blue. Using two Gaussian functions to fit the population distribution in Fig. 7 and considering that the high and low frequency components correspond to the free and complex forms, respectively, we found that the equilibrium constant $[\text{complex}]_{eq}/[\text{free}]_{eq}$ to be about 2.7—note that the experimental value is ~ 1.[4]

From the time dependence of the OD stretch frequency, one can readily calculate the FFCF, defined as

$$C_\omega(t) = \langle (\omega_{OD}(t) - \langle \omega_{OD} \rangle)(\omega_{OD}(0) - \langle \omega_{OD} \rangle) \rangle, \tag{4}$$

where the average frequency is found to be 2641.7 cm^{-1}. Although FFCF would not be used to numerically calculate the linear and nonlinear vibrational response functions for the 1D and 2D IR spectroscopies, it will be directly compared with the fluctuations of the inhomogeneously distributed solvent environments around the phenol molecule in the following section. In Fig. 8 the numerically calculated $C_\omega(t)$ (solid curve) is plotted. The dashed curve is a biexponential fit to $C_\omega(t)$ obtained from the simulations, i.e.,

$$C_\omega(t) = A_1 \exp(-t/\tau_1) + A_2 \exp(-t/\tau_2), \tag{5}$$

where $A_1 = 138\ \text{cm}^{-2}$, $\tau_1 = 0.34$ ps, $A_2 = 220\ \text{cm}^{-2}$, and $\tau_2 = 5.35$ ps. The biexponential does a good job of reproducing the curve and gives a convenient analytical form which will be used later. As will be discussed below, the slow component with $\tau_2 = 5.35$ ps is directly associated with the dynamic equilibrium process between the free and complex forms of phenol in the benzene/CCl_4 solution.

B. Configuration and frequency-dependent OD stretch transition dipole moment

The OD transition dipole moment was shown to be strongly dependent on the local environment. It was determined experimentally that the transition dipole of the

phenol-benzene complex is about 1.5 times larger than that of the free phenol.[4] Here, the free phenol approximately corresponds to the case when the phenol is surrounded by CCl_4 molecules. In a real solution, the phenol molecule can have varying local solvation configurations that are neither a perfect complex form nor a perfect free form. Therefore, it is necessary to develop a theoretical method that can be used to quantitatively determine the OD transition dipole moment for a given instantaneous configuration sampled from the MD trajectories. An alternative is to find a relationship between the OD stretch frequency and the transition dipole moment. It should be noted that the OD stretch frequency reflects the surrounding solvent configuration, as can be inferred from eqs. (2) and (3). It is a reasonable assumption that the transition dipole moment of the OD stretch when the phenol is in solution is a function of the electric field along the OD bond, i.e.,

$$\mu_{\mathrm{OD}}(E) \cong \mu_f + \left(\frac{\partial \mu_{\mathrm{OD}}}{\partial E}\right)_0 E, \tag{6}$$

where μ_f is the transition dipole moment of the free phenol (μ_f=0.96 D Å^{-1} amu$^{-1/2}$ at MP2/cc-pVDZ). Inserting Eq. (2) into Eq. (6), we find

$$\mu_{\mathrm{OD}}(\omega_{\mathrm{OD}}) \cong \mu_f + \frac{1}{\kappa}\left(\frac{\partial \mu_{\mathrm{OD}}}{\partial E}\right)_0 (\omega_{\mathrm{OD}} - \omega_{\mathrm{OD}}^0). \tag{7}$$

In order to determine the linear expansion coefficient, $(\partial\mu_{\mathrm{OD}}/\partial E)_0$, we chose the phenol-benzene complex with the geometry optimized using the MP2/6-31G* method. Employing the FF partial charges of the benzene molecule, which were used to run the MD simulations, we calculated the E and μ_{OD} values for the configuration that was determined with the QM calculation. We then find $(\partial\mu_{\mathrm{OD}}/\partial E)_0$ to be 52.7 D Å^{-1} amu$^{-1/2}$(a.u. E)$^{-1}$. Here it is noted that the experimentally measured transition dipole ratio μ_c/μ_f is ~1.5. Within the assumption that the transition dipole moment of the free phenol is μ_f=0.96 D Å^{-1} amu$^{-1/2}$, we find that the experimentally estimated $(\partial\mu_{\mathrm{OD}}/\partial E)_0$ value is about 60 D Å^{-1} amu$^{-1/2}$(a.u. E)$^{-1}$. In the following numerical simulations of IR absorption and 2D IR spectra, we will use the theoretically calculated value for $(\partial\mu_{\mathrm{OD}}/\partial E)_0$.

C. The OD stretch absorption spectrum

The absorption line shape function is given by the Fourier transform of the quantum mechanical dipole correlation function as[3]

$$I(\omega) \sim \int_{-\infty}^{\infty} dt e^{i\omega t}\langle \mu(t)\cdot\mu(0)\rangle, \tag{8}$$

where μ denotes the quantum mechanical dipole operator. $I(\omega)$ can be rewritten in terms of the linear response function $J(t)$,[83]

$$I(\omega) \sim |\mu_{\mathrm{OD}}(\omega)|^2 \int_{-\infty}^{\infty} dt e^{i\omega t}\bar{J}(t), \tag{9}$$

where $\bar{J}(t)=J(t)C_1(t)\exp(-i<\omega_{10}>t)$, and

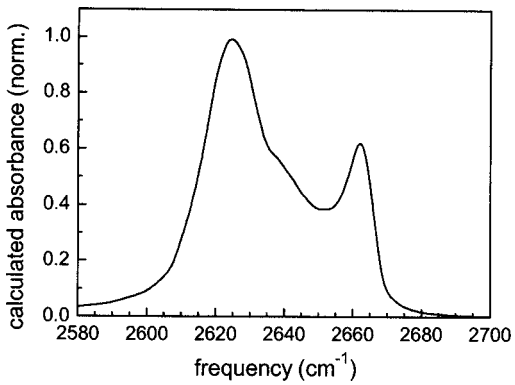

FIG. 9. Calculated OD stretch absorption spectrum.

$$J(t) \equiv \left\langle \exp_+\left[-i\int_0^t d\tau \delta\hat{\omega}_{10}(\tau)\right]\right\rangle. \tag{10}$$

Here, $\delta\hat{\omega}_{10}(\tau)$ is the fluctuating angular frequency operator in the Heisenberg representation. $\langle\cdots\rangle$ is, in this case, the quantum mechanical trace over the bath eigenstates. $C_1(t)$ is the first-order rotational correlation function that describes the rotational relaxation of the phenol molecule in solution and is defined as $C_1(t)=\langle P_1(\cos\theta(t))\rangle$, where P_1 is the first-order Legendre polynomial and $\theta(t)$ is the angle between the dipole vector at time zero and that at time t. As is the standard practice, vibration-rotation coupling effects are ignored.[83] As discussed above, the configuration-dependent transition dipole moment is taken into account through the use of Eq. (7).

Because the OD stretch frequency distribution is not Gaussian, one cannot use the second-order truncated cumulant expansion technique[83] to calculate the linear response function, $J(t)$. Therefore, we instead use a classical ensemble averaging method.[59] The linear response function in Eq. (10) is approximated as

$$J_c(t) = \left\langle \exp\left[-i\int_0^t d\tau \delta\omega_{10}(\mathbf{q},\mathbf{p},\tau)\right]\right\rangle_c, \tag{11}$$

where the fluctuating part of the frequency is replaced with a classical function, i.e., $\delta\omega_{10}=\delta\omega_{\mathrm{OD}}=\omega_{\mathrm{OD}}-\langle\omega_{\mathrm{OD}}\rangle_c$, in the phase space of the bath degrees of freedom.

The lifetime broadening effect, which is very small, is taken into account by using the normal approach,

$$J_c(t) \to J_c(t)\exp(-t/2T_1), \tag{12}$$

where the lifetime of the first excited state is taken to be 11 ps, which is approximately the average of the lifetime of the complex (10 ps) and the lifetime of free phenol (12.5 ps).[4]

Figure 9 displays the OD stretch absorption spectrum obtained from the simulations. The calculated spectrum

should be compared to the experimental spectrum displayed in Fig. 1(a). The peak positions are close to correct. The calculated peak positions are compared to the experimental values of 2631 and 2665 cm^{-1}. The peak for the complex is wider than for the free phenol, as is true of the experimental spectrum. However, the calculation yields a band for the complex that is somewhat too large relative to the size of the free phenol band. In addition, the calculated spectrum displays a shoulder between the two bands that is not evident in the experiment. However, the shoulder may be obscured in the experiment by the much large size of the free phenol peak. Given the complexity of the system involving two species, the complexed and free phenol, and the large range of local solvent environment, which are discussed in detail below, the agreement between the experimental and calculated spectra is reasonably good.

D. 2D vibrational echoes: Theory

The nonlinear response functions that are directly associated with 2D IR spectroscopy have been presented and discussed in detail.[84] As mentioned above, the frequency distribution of the OD stretch deviates strongly from a Gaussian function so that it is not possible to use the same second-order cumulant approximate expressions. Therefore, to calculate the corresponding nonlinear response functions denoted as $\Phi_j(t_3,t_2,t_1)$,[59,84] we will employ the ensemble averaging procedure used to calculate the linear response function in Sec. IV C. Furthermore, we will assume that $\delta\omega_{21}(t)=\delta\omega_{10}(t)$, which is the harmonic approximation.[60] Then, we have

$$\begin{aligned}
\Phi_1(t_3,t_2,t_1) &= -2\exp\{-i\langle\omega_{21}\rangle t_3 + i\langle\omega_{10}\rangle t_1\} \\
&\quad\times\Psi_A(t_3,t_2,t_1)\Gamma_{\mathrm{TA}}(t_3,t_2,t_1)Y(t_3,t_2,t_1), \\
\Phi_2(t_3,t_2,t_1) &= -2\exp\{-i\langle\omega_{21}\rangle t_3 - i\langle\omega_{10}\rangle t_1\} \\
&\quad\times\Psi_B(t_3,t_2,t_1)\Gamma_{\mathrm{TA}}(t_3,t_2,t_1)Y(t_3,t_2,t_1), \\
\Phi_3(t_3,t_2,t_1) &= \exp\{-i\langle\omega_{10}\rangle t_3 + i\langle\omega_{10}\rangle t_1\} \\
&\quad\times\Psi_A(t_3,t_2,t_1)\Gamma_{\mathrm{SE}}(t_3,t_2,t_1)Y(t_3,t_2,t_1), \\
\Phi_4(t_3,t_2,t_1) &= \exp\{-i\langle\omega_{10}\rangle t_3 - i\langle\omega_{10}\rangle t_1\} \\
&\quad\times\Psi_B(t_3,t_2,t_1)\Gamma_{\mathrm{SE}}(t_3,t_2,t_1)Y(t_3,t_2,t_1), \\
\Phi_5(t_3,t_2,t_1) &= \exp\{-i\langle\omega_{10}\rangle t_3 + i\langle\omega_{10}\rangle t_1\} \\
&\quad\times\Psi_A(t_3,t_2,t_1)\Gamma_{\mathrm{GB}}(t_3,t_2,t_1)Y(t_3,t_2,t_1), \\
\Phi_6(t_3,t_2,t_1) &= \exp\{-i\langle\omega_{10}\rangle t_3 - i\langle\omega_{10}\rangle t_1\} \\
&\quad\times\Psi_B(t_3,t_2,t_1)\Gamma_{\mathrm{GB}}(t_3,t_2,t_1)Y(t_3,t_2,t_1),
\end{aligned} \tag{13}$$

where the dephasing-induced line broadening factors, $\Psi_A(t_3,t_2,t_1)$ and $\Psi_B(t_3,t_2,t_1)$, are defined as

$$\begin{aligned}
\Psi_A(t_3,t_2,t_1) &\equiv \left\langle \exp\left\{ i\int_0^{t_1} d\tau\delta\omega_{10}(\tau)\right\}\right. \\
&\quad\left.\times\exp\left\{ -i\int_{t_1+t_2}^{t_1+t_2+t_3} d\tau\delta\omega_{10}(\tau)\right\}\right\rangle, \\
\Psi_B(t_3,t_2,t_1) &\equiv \left\langle \exp\left\{ -i\int_0^{t_1} d\tau\delta\omega_{10}(\tau)\right\}\right. \\
&\quad\left.\times\exp\left\{ -i\int_{t_1+t_2}^{t_1+t_2+t_3} d\tau\delta\omega_{10}(\tau)\right\}\right\rangle.
\end{aligned} \tag{14}$$

The first two contributions, $\Phi_1(t_3,t_2,t_1)$ and $\Phi_2(t_3,t_2,t_1)$, describe the induced transient absorption (TA) between the $v=1$ state and the $v=2$ state, $\Phi_3(t_3,t_2,t_1)$ and $\Phi_4(t_3,t_2,t_1)$ are associated with the stimulated emission (SE) process where the excited state ($v=1$) population evolution is involved, and finally $\Phi_5(t_3,t_2,t_1)$ and $\Phi_6(t_3,t_2,t_1)$ are associated with the ground-state bleaching (GB) contribution where a hole created on the ground state ($v=0$) evolves in time during the population period, t_2. Here, the transition dipole product term was not included in Eq. (13), and the configuration-dependent transition dipole moment will be taken into consideration later in Eq. (19) when the 2D IR spectrum is calculated. The factor of 2 in $\Phi_1(t_3,t_2,t_1)$ and $\Phi_2(t_3,t_2,t_1)$ is included because these contributions involve vibrational transition from the first excited state to the second excited state (two interactions with the radiation field) and within the harmonic approximation the transition dipole for this transition is $\sqrt{2}$ bigger than the $v=0$ to $v=1$ transition dipole.

Denoting the inverse lifetimes of the first and second excited states as γ_1 and γ_2, respectively, we find that the lifetime-broadening factors in Eqs. (13) are given as

$$\begin{aligned}
\Gamma_{\mathrm{TA}}(t_3,t_2,t_1) &= \exp\left\{ -\frac{(\gamma_1+\gamma_2)t_3}{2} - \gamma_1 t_2 - \frac{\gamma_1 t_1}{2}\right\}, \\
\Gamma_{\mathrm{SE}}(t_3,t_2,t_1) &= \exp\left\{ -\frac{\gamma_1 t_3}{2} - \gamma_1 t_2 - \frac{\gamma_1 t_1}{2}\right\}, \\
\Gamma_{\mathrm{GB}}(t_3,t_2,t_1) &= \exp\left\{ -\frac{\gamma_1 t_3}{2} - \gamma_1 t_2 - \frac{\gamma_1 t_1}{2}\right\}.
\end{aligned} \tag{15}$$

The lifetimes of the first excited state of the complex and the free phenol were determined experimentally.[4] As discussed above, a value of 11 ps is used. Within the harmonic approximation, the lifetime of the second excited state is a factor of 2 shorter. This approximation is adequate because the lifetime is much longer than the coherence period, t_3.

Finally, the rotational relaxation of phenol molecule in solution contributes to the total nonlinear response function and it is taken into consideration by the auxiliary function $Y(t_3,t_2,t_1)$, defined as[85,86]

$$Y(t_3,t_2,t_1) = \tfrac{1}{9}C_1(t_3)C_2(t_2)C_1(t_1), \tag{16}$$

where $C_1(t_i)$ was previously defined and

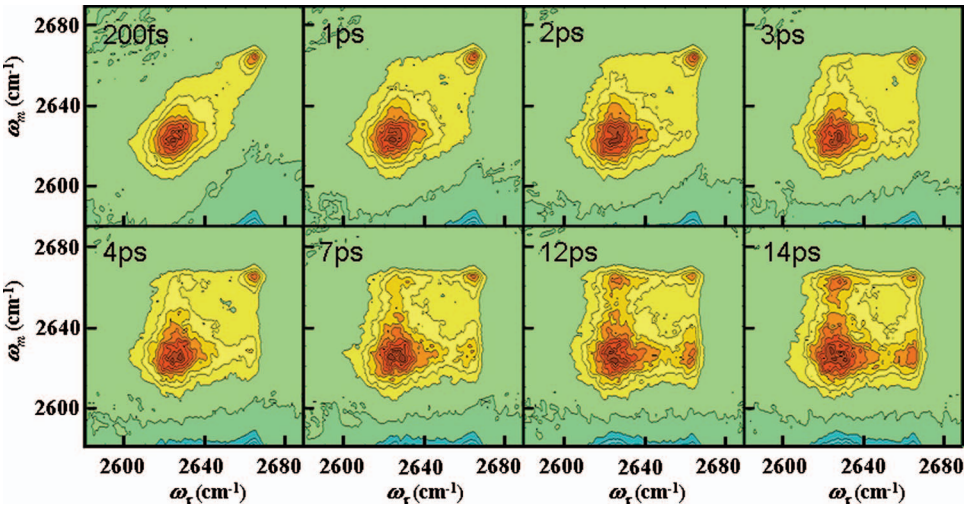

FIG. 10. (Color) 2D vibrational echo spectra calculated from the MD simulations. As T_w increases the off-diagonal chemical exchange peaks grow in. Compared to the experimental results shown in Figs. 1(b) and 1(c).

$$C_2(t_2) = \left(1 + \tfrac{4}{5}\langle P_2(\cos\,\theta(t_2))\rangle\right). \tag{17}$$

Here, $P_2(x)$ is the second-order Legendre polynomial. In the present numerical simulation of 2D IR spectra, we shall use $C_1(t_i)$ and $C_2(t_2)$ in the inset of Fig. 8, which were obtained from MD trajectories.

To quantitatively determine the 2D IR vibrational echo spectra including chemical exchange between the complex and free phenol, the two dephasing-induced line broadening factors, $\Psi_A(t_3,t_2,t_1)$ and $\Psi_B(t_3,t_2,t_1)$, defined in Eq. (14) are calculated from the MD trajectories. Once these three-dimensional functions, $\Psi_A(t_3,t_2,t_1)$ and $\Psi_B(t_3,t_2,t_1)$, lifetime broadening factors, and rotational relaxation terms are determined, the 2D spectra are obtained using[59]

$$\tilde{\Phi}_j(\omega_1,\omega_3;\tau) = \int_0^\infty dt_3 \int_0^\infty dt_1 \exp(i\omega_3 t_3 - i\omega_1 t_1) \times \Phi_j(t_3, t_2=\tau, t_1) \quad (\text{for } j=1,3, \text{ and } 5),$$
$$\tilde{\Phi}_k(\omega_1,\omega_3;\tau) = \int_0^\infty dt_3 \int_0^\infty dt_1 \exp(i\omega_3 t_3 + i\omega_1 t_1) \times \Phi_k(t_3, t_2=\tau, t_1) \quad (\text{for } k=2,4, \text{ and } 6). \tag{18}$$

Here the 2D vibrational echo spectrum, $S_{2D}(\omega_1,\omega_3;\tau)$, is defined as

$$S_{2D}(\omega_1,\omega_3;\tau) = |\mu_{OD}(\omega_1)|^2 |\mu_{OD}(\omega_3+\Delta)|^2 \times \mathrm{Re}\left[\sum_{i=1}^{2} \tilde{\Phi}_i(\omega_1,\omega_3;\tau)\right] + |\mu_{OD}(\omega_1)|^2 |\mu_{OD}(\omega_3)|^2 \times \mathrm{Re}\left[\sum_{i=3}^{6} \tilde{\Phi}_i(\omega_1,\omega_3;\tau)\right], \tag{19}$$

where Δ is the overtone anharmonicity frequency of 91 cm^{-1}. The configuration-dependent transition dipole is considered in this expression. Note that the transition dipole depends on local solvation environment through E (electric field). And then, using the relation between OD stretch mode frequency and E, we can find the frequency-dependent transition dipole moment. Here, the prefactor, $|\mu_{OD}(\omega_1)|^2|\mu_{OD}(\omega_3)|^2$, approximately describes the configuration-dependent transition dipole moment in the context of 2D IR nonlinear response function.

E. Simulated 2D vibrational echo spectra and comparison to experiment

Figure 10 displays the 2D vibrational echo spectra calculated from the simulations as described above. The plots display the $v=0-1$ regions of the spectrum. At the shortest T_w (time between pulses 2 and 3), there are only peaks on the diagonal. As T_w increases off-diagonal peaks grow in. The increase in these peaks reflects the chemical exchange in which complexes are formed and dissociate.[59] The spectra at the shortest and longest T_w's can be compared to the experimental data[4] shown in Figs. 1(b) and 1(c). The plots in Fig. 10 capture the main features of the experimental data. However, the peak on the diagonal associated with the complex (ω_m=2630cm^{-1}) is too large compared to the diagonal free peak (ω_m=2663cm^{-1}) when compared to the experimental results. This is not a failure of the methodology for calculating the nonlinear signal, but rather it is in accord with the equilibrium constant of 2.7 rather than the experimental value of 1 and the linear spectrum which shows that the size of the band for the phenol-benzene complex relative to that for free phenol is too large compared to the experimental spectrum [see Figs. 9 and 1(a)].

It is difficult to compare the calculated and experimental chemical exchange dynamics by comparing the 2D plots directly. This is particularly true because the peak heights are influenced by spectral diffusion, which causes the widths of the peaks to increase and their amplitudes to decrease. However, spectral diffusion does not change the peak volumes. Only population dynamics change the peak volumes. It has been demonstrated that the peak volumes can be used to extract the chemical exchange dynamics.[6] The vibrational relaxation to the ground state and orientational relaxation cause all of the peaks to decrease, while chemical exchange causes the diagonal peaks to decrease but the off-diagonal peaks to grow in. The calculations include all three contributions to the peak volumes. Figures 11(a) and 11(b) show the

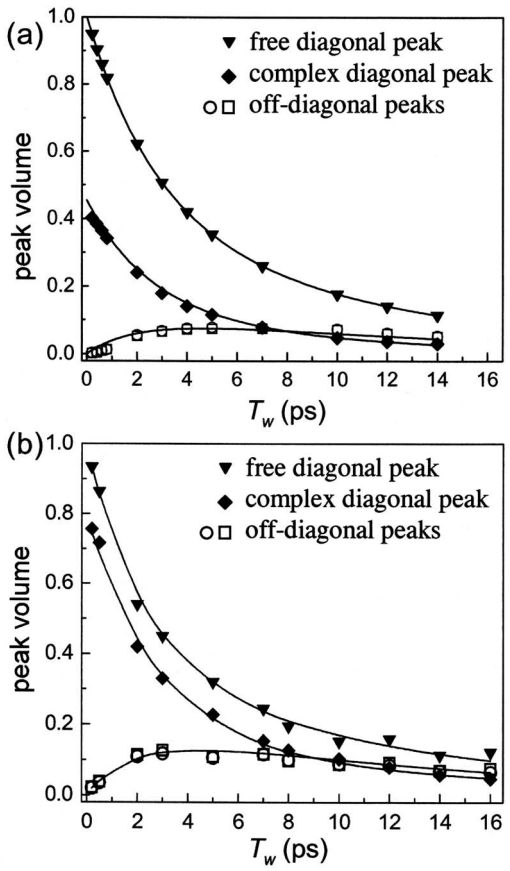

FIG. 11. Calculated (a) and experimental (b) diagonal and off-diagonal peak volumes. The peaks on the diagonal arise from the free phenol (higher frequency) and the phenol-benzene complex (lower frequency). The off-diagonal peaks are formed by formation and dissociation of the complex.

calculated and experimental T_w dependent peak volumes, respectively. The lines through the calculated and experimental data used a single adjustable parameter in the fits, the complex dissociation time, τ_d, which is the inverse of the complex dissociation rate. As discussed in the introduction, $\tau_d = 8$ ps from the experimental fits. In the experiments the orientational relaxation rates, the lifetimes, the ratio of the transition dipole for the two peaks, and the equilibrium constant were all measured separately and used as input parameters. In the calculations, the lifetime was taken from the experiments but everything else including the configuration-dependent transition dipole, the orientational relaxation, and the equilibrium between the complex and free phenol are contained in the simulation. These factors determine not only the time dependence of the peaks but the relative amplitudes of the peaks as a function of time. While not perfect, the simulations do a respectable job reproducing the chemical exchange and the other dynamics of the system.

From the simulations and using the theory in Ref. 61 and the fitting procedure used previously to analyze the experimental data,[4–6] we found that the dissociation time constant τ_d is 20 ps, which is two and a half times larger than the experimental value of 8 ps. This value of τ_d is somewhat too slow, but given the complexity of the problem, the simulation describes the system characteristics almost quantitatively. The value of the dissociation time is consistent with the value for the equilibrium $[\text{complex}]_{eq}/[\text{free}]_{eq} = 2.7$ found in this study. The equilibrium constant is too large compared to experiment and the dissociation time is too slow. Both indicate that the classical force field used in the simulations overestimates the strength of the phenol-benzene complex bond.

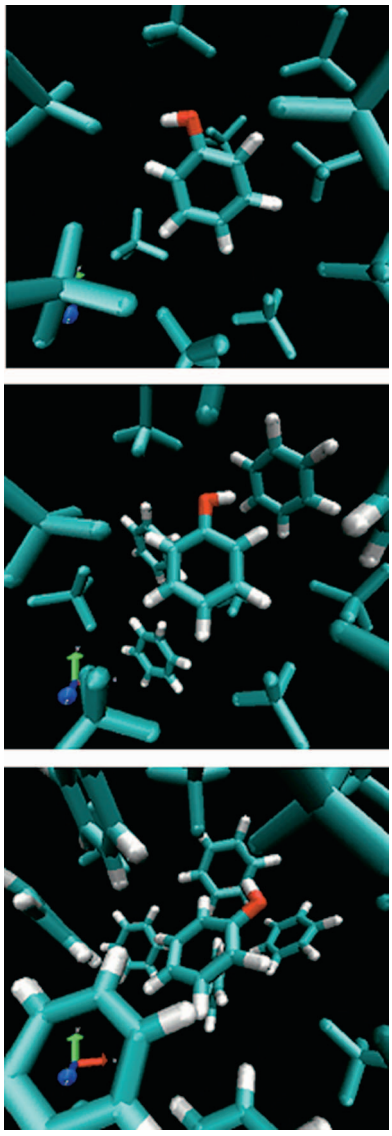

FIG. 12. (Color) Representative configurations extracted from the simulations. Top panel: free phenol surrounded by CCl_4 molecules ($X_b \sim 0$). Middle panel: phenol-benzene complex surrounded by a mix of benzene and CCl_4 molecule ($X_b \sim 0.5$). Bottom panel: phenol-benzene complex surrounded mainly by benzene molecules ($X_b \sim 1$).

V. LOCAL SOLVATION ENVIRONMENT AND RELAXATION

From the MD simulation trajectories, three representative snapshot configurations are shown in Fig. 12. The top panel shows the situation where the free phenol molecule is predominantly surrounded by CCl_4 molecules ($X_b \sim 0$). The middle panel shows a phenol-benzene complex surrounded by a mix of benzene and CCl_4 molecules ($X_b \sim 0.5$), and the bottom panel shows a complex with the surrounding molecules mainly benzenes ($X_b \sim 1$). This suggests that the

benzene//CCl_4 mixed solution is not homogeneous at the level of the solute molecule, in this case, phenol and that microscopic solvent domains that are rich in benzene or CCl_4 can exist in this mixed solution. Then, the free-complex dynamical equilibrium process in part involves phenol changing between locally inhomogeneous solvent environments. The chemical exchanges between complex and free phenol are directly probed in the 2D IR spectroscopic measurements. However, another issue that is interesting to study is the local solvation dynamics and inhomogeneity of the local environments around the solute in the mixed solvent. Such dynamics gives rise to spectral diffusion.

Recently an initial experimental analysis of the spectral diffusion of the complex and the free phenol was performed on the benzene phenol system.[6] However, the extraction of the FFCFs of the two species is complicated by the chemical exchange process.[6] Additional experiments are underway on a similar system in which the chemical exchange is much slower than the spectral diffusion, which will greatly simplify the analysis of the spectral diffusion.[87] Here we will address the issue of extracting information on the fluctuation of solvent molecules within the first solvation shell around the solute from vibrational echo spectroscopy. The question arises as to which observable or correlation function can be used to retrieve information on the number of solvent molecules in the vicinity of the solute. In the present section, we will provide a line of theoretical reasoning and plausible answers to these interesting questions.

A. Statistical aspects

To establish the connection between the distribution of microscopically inhomogeneous environments and the spectroscopically measurable OD stretch frequency, we have analyzed the MD trajectories and examined the solvent molecular distribution around the phenol OD chromophore. From the phenol in benzene and phenol in CCl_4 solutions, we calculated the radial distribution functions. We found that the average radius of the first solvation shell is about 5 Å from the center of mass of the phenol OD bond. Now, for the phenol in benzene/CCl_4 solution, we separately counted the number of benzene and CCl_4 molecules within the sphere around the OD bond with a radius of 5 Å. The two numbers are denoted as N_b and N_c. If the center of mass of solvent molecule is inside this solvation shell, that molecule is counted. We found that the average values, $\langle N_b \rangle$ and $\langle N_c \rangle$, are 1.166 and 1.319, respectively. The local number fraction of benzene molecule is then defined as

$$X_b(t) = \frac{N_b(t)}{N_b(t) + N_c(t)}. \tag{20}$$

This value fluctuates in time, and its magnitude is a measure of local inhomogeneity of the solvent molecules in the first solvation shell. $X_b(t)$ differs from the macroscopic mole fraction that is constant in time. Dynamical relaxation of the variables, $X_b(t)$, $N_b(t)$, and $N_c(t)$, will be discussed later in this section.

Because the numbers of benzene and CCl_4 molecules in the first solvation shell are finite and typically less than 5 for benzene and 6 for CCl_4, X_b values are discrete (see Table IV). The probability distribution of X_b can be obtained from the MD trajectories, and it is plotted in Fig. 13(a). Surprisingly, the distribution is not uniform nor symmetric around the value of macroscopic mole fraction of benzene, ~0.29. If we considered a sphere with much larger radius and count the number of included benzene and CCl_4 molecules within the sphere, the distribution obtained would been broad and close to normal distribution with maximum at ~0.29. In Table IV, the probabilities in percent for varying X_b are summarized. Among these, the most probable X_b value is 0.5, which is larger than the macroscopic benzene mole fraction of 0.286. Furthermore, the probabilities of finding X_b value to be 0.333, 0.667, and 1 are 17.5%, 11.8%, and 20.5%, respectively. This observation suggests (1) that the local sol-

TABLE IV. Local number fraction of benzene molecules X_b and its probability (%).

X_b	Probability (%)
0	15.7
0.2	0.2
0.25	3.9
0.333	17.5
0.4	0.3
0.5	28.7
0.6	0.1
0.667	11.8
0.75	1.2
0.8	0.03
1	20.5

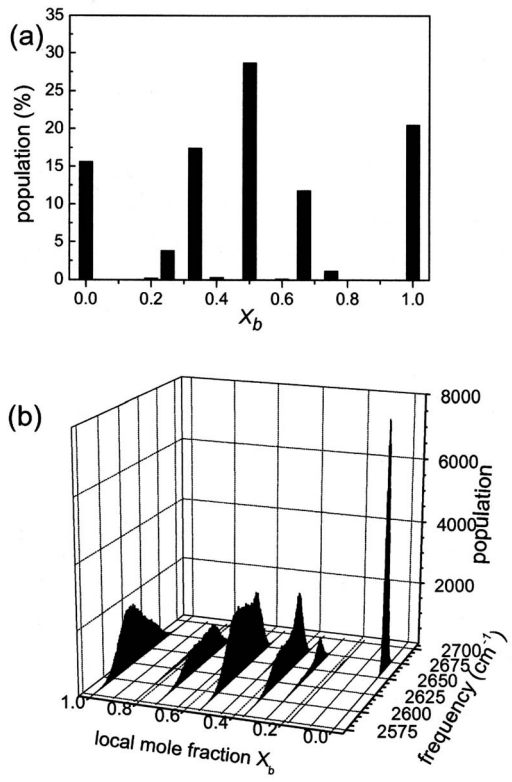

FIG. 13. (a) Population distribution of X_b. (b) Population distribution with respect to X_b and OD stretch mode frequency.

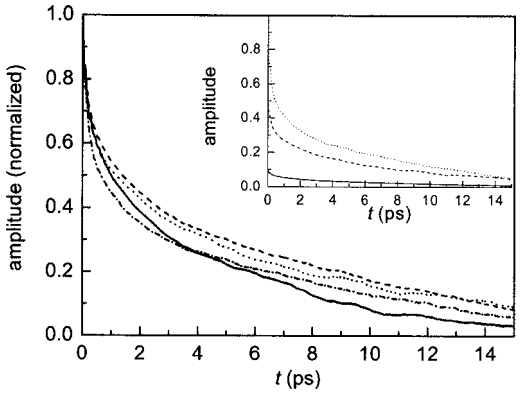

FIG. 14. Normalized correlation functions, $C_{\delta X_b}(t)/C_{\delta X_b}(0)$ (dashed line), $C_{\delta N_b}(t)/C_{\delta N_b}(0)$ (dotted line), and $C_{\delta N_c}(t)/C_{\delta N_c}(0)$ (dash-dotted line), and the normalized OD stretch mode frequency-frequency correlation function, $C_\omega(t)/C_\omega(0)$ (solid line). In the inset, $C_{\delta X_b}(t)$ (solid line), $C_{\delta N_b}(t)$ (dashed line), and $C_{\delta N_c}(t)$ (dotted line).

vation environment in the first solvation shell around the phenol is fairly different from the bulk, (2) that each solute phenol has a discretely different inhomogeneous solvation structure at a given time, and (3) that the phenol is preferentially solvated by benzene. In addition, two limiting cases of $X_b=0$ and $X_b=1$ significantly populate, indicating that the two different solvent molecules can approximately form microscopic domains at least in the vicinity of the phenol, where by microscopic domain we mean a local region where one solvent species is predominantly rich in number.

To find the correlation between X_b and OD stretch mode frequency, we obtained the distributions of the OD frequencies for each X_b. These are plotted in Fig. 13(b). If $X_b=0$, the OD frequency distribution is quite narrow, and its center is around 2670 cm^{-1}. As X_b increases, the distribution becomes broad and its maximum position gradually shifts to lower frequency, as expected.

B. Dynamical aspects

We next consider relaxation dynamics of variables such as $X_b(t)$, $N_b(t)$, and $N_c(t)$, which are reflections of the local solvation environments. In the inset of Fig. 14, the correlation functions $C_{\delta X_b}(t)$ (red), $C_{\delta N_b}(t)$ (blue), and $C_{\delta N_c}(t)$ (green) are plotted, where

$$C_{\delta X_b}(t) = \langle (X_b(t) - \langle X_b \rangle)(X_b(0) - \langle X_b \rangle) \rangle,$$

$$C_{\delta N_b}(t) = \langle (N_b(t) - \langle N_b \rangle)(N_b(0) - \langle N_b \rangle) \rangle, \quad (21)$$

$$C_{\delta N_c}(t) = \langle (N_c(t) - \langle N_c \rangle)(N_c(0) - \langle N_c \rangle) \rangle.$$

All three correlation functions have a fast and slow decay component, though their initial values differ from one another. To more readily compare the decays of the correlation functions, the normalized correlation functions are plotted in the main part of Fig. 14. As can be seen in the figure, the decays of the three correlation functions are very similar. Furthermore, the normalized FFCF, $C_\omega(t)$ [see Eq. (4)], is also plotted in Fig. 14 as the black curve and found to be quite close to the normalized correlation functions of the local concentrations in the first solvation shell. This observation is quite important because one might be able to use the experimentally measurable $C_\omega(t)/C_\omega(0)$ function to infer the local solvent dynamics in the first solvation shell, for example, $C_{\delta X_b}(t)/C_{\delta X_b}(0)$.

On the basis of the empirical observations made from Fig. 14,

$$C_\omega(t)/C_\omega(0) \approx C_{\delta X_b}(t)/C_{\delta X_b}(0) \approx C_{\delta N_b}(t)/C_{\delta N_b}(0), \quad (22)$$

we propose the following ansatz. There is a simple relationship between the projected electric field E and the number of benzene molecules in the first solvation shell, i.e.,

$$E = \gamma N_b. \quad (23)$$

Then, we have, from Eqs. (2) and (23),

$$C_\omega(t) = \kappa^2 \gamma^2 C_{\delta N_b}(t). \quad (24)$$

Here, the proportionality constant γ is estimated to be 0.0065 a.u. E/benzene, where the electric field component is in a.u. The relationship in Eq. (24) suggests that by measuring the FFCF one can directly extract information on the solvent molecule concentration dynamics in the immediate vicinity of the solute phenol.

VI. CONCLUDING REMARKS

In this paper MD simulations were used to examine the dynamics of phenol in the mixed benzene/CCl_4 solvent. As has been well documented experimentally, phenol forms a complex with benzene, and at room temperature under thermal equilibrium conditions, the complexes are continually forming and dissociating.[4,6] Ultrafast 2D vibration echo experiments have been used to directly measure the chemical exchange between phenol in the complex and free forms. Although the exchange kinetics can be accurately determined from experiments, the experiments do not provide a microscopic picture of the formation and dissociation process.

The combination of the experimental results and the MD simulations amplify both approaches to understand solute-solvent complexes and the nature of solute interactions in complex solvent environments. The experimental results provide benchmarks for the simulations. The calculations of two types of observables from the MD simulations demonstrate that the simulations are of sufficient accuracy to produce usable insights into the details of the system. The simulations were able to do a reasonable job of reproducing both the linear IR absorption spectrum of the phenol hydroxyl stretch and the time-dependent 2D vibrational echo spectra. Of particular importance is that the simulations produced reasonable agreement with the determination of the experimentally measured complex dissociation time.

Perhaps the most interesting feature of the simulation results is the description of the number distribution of solvent molecules in the first solvation shell of the phenol. The number of benzenes on average was not the mole fraction of benzene in the solvent. Furthermore, as shown in Fig. 13, the number distribution of benzenes and CCl_4 in the first solvent shell is highly inhomogeneous. In fact, there are significant probabilities of finding a phenol surrounded either completely by benzene or completely by CCl_4. Furthermore, it

was proposed that the time dependence of the inhomogeneous nature of the solvent environment about the solute can be probed experimentally through the 2D vibrational experiments using a relationship between the fraction of benzenes in the first solvation shell and the frequency-frequency correlation function.

ACKNOWLEDGMENTS

Three of the authors (K.K., J.Z., and M.D.F.) would like to thank the United States Air Force Office of Scientific Research (F49620-01-1-0018) for supporting their contribution to this research. Another author (M.C.) thanks for the financial support from CRIP of MOST, Korea.

[1] C. J. Cramer and D. G. Truhlar, Chem. Rev. (Washington, D.C.) **99**, 2161 (1999).
[2] J. Hansen and I. McDonald, *Theory of Simple Liquids* (Academic, London, 1976).
[3] D. McQuarrie, *Statistical Mechanics* (Harper & Row, New York, 1976).
[4] J. Zheng, K. Kwak, J. Asbury, X. Chen, I. R. Piletic, and M. D. Fayer, Science **309**, 1338 (2005).
[5] J. Zheng, K. Kwak, X. Chen, J. B. Asbury, and M. D. Fayer, J. Am. Chem. Soc. **128**, 2977 (2006).
[6] K. Kwak, J. Zheng, H. Cang, and M. D. Fayer, J. Phys. Chem. B **110**, 19998 (2006).
[7] H. J. Bakker, H. K. Neinhuys, G. Gallot, N. Lascoux, G. M. Gale, J. C. Leicknam, and S. Bratos, J. Chem. Phys. **116**, 2592 (2002).
[8] M. F. Kropman, H.-K. Nienhuys, S. Woutersen, and H. J. Bakker, J. Phys. Chem. A **105**, 4622 (2001).
[9] M. F. Kropman and H. J. Bakker, J. Chem. Phys. **115**, 8942 (2001).
[10] S. Woutersen and H. J. Bakker, Comments Mod. Phys. **2**, D99 (2000).
[11] H. J. Bakker, S. Woutersen, and H. K. Nienhuys, Chem. Phys. **258**, 233 (2000).
[12] C. J. Fecko, J. D. Eaves, J. J. Loparo, A. Tokmakoff, and P. L. Geissler, Science **301**, 1698 (2003).
[13] C. J. Fecko, J. J. Loparo, S. T. Roberts, and A. Tokmakoff, J. Chem. Phys. **122**, 054506 (2005).
[14] J. B. Asbury, T. Steinel, and M. D. Fayer, J. Lumin. **107**, 271 (2004).
[15] S. Yeremenko, M. S. Pshenichnikov, and D. A. Wiersma, Chem. Phys. Lett. **369**, 107 (2003).
[16] S. Yeremenko, M. S. Pshenichnikov, and D. A. Wiersma, Phys. Rev. A **73**, 021804 (2006).
[17] J. D. Eaves, A. Tokmakoff, and P. L. Geissler, J. Phys. Chem. A **109**, 9424 (2005).
[18] J. D. Eaves, J. J. Loparo, C. J. Fecko, A. Tokmakoff, and P. L. Geissler, Proc. Natl. Acad. Sci. U.S.A. **102**, 13019 (2005).
[19] T. Steinel, J. B. Asbury, S. A. Corcelli, C. P. Lawrence, J. L. Skinner, and M. D. Fayer, Chem. Phys. Lett. **386**, 295 (2004).
[20] S. Corcelli, C. P. Lawrence, J. B. Asbury, T. Steinel, M. D. Fayer, and J. L. Skinner, J. Chem. Phys. **121**, 8897 (2004).
[21] J. B. Asbury, T. Steinel, C. Stromberg, S. A. Corcelli, C. P. Lawrence, J. L. Skinner, and M. D. Fayer, J. Phys. Chem. A **108**, 1107 (2004).
[22] J. B. Asbury, T. Steinel, K. Kwak, S. Corcelli, C. P. Lawrence, J. L. Skinner, and M. D. Fayer, J. Chem. Phys. **121**, 12431 (2004).
[23] M. Bonn, H. J. Bakker, A. W. Kleyn, and R. A. van Santen, J. Phys. Chem. **100**, 15301 (1996).
[24] S. Woutersen, U. Emmerichs, and H. J. Bakker, J. Chem. Phys. **107**, 1483 (1997).
[25] M. A. F. H. van den Broek, H. K. Nienhuys, and H. J. Bakker, J. Chem. Phys. **114**, 3182 (2001).
[26] K. Gaffney, I. Piletic, and M. D. Fayer, J. Phys. Chem. A **106**, 9428 (2002).
[27] K. J. Gaffney, P. H. Davis, I. R. Piletic, N. E. Levinger, and M. D. Fayer, J. Phys. Chem. A **106**, 12012 (2002).
[28] J. B. Asbury, T. Steinel, C. Stromberg, K. J. Gaffney, I. R. Piletic, A. Goun, and M. D. Fayer, Chem. Phys. Lett. **374**, 362 (2003).
[29] J. B. Asbury, T. Steinel, C. Stromberg, K. J. Gaffney, I. R. Piletic, A. Goun, and M. D. Fayer, Phys. Rev. Lett. **91**, 237402 (2003).
[30] J. B. Asbury, T. Steinel, C. Stromberg, K. J. Gaffney, I. R. Piletic, and M. D. Fayer, J. Chem. Phys. **119**, 12981 (2003).
[31] K. J. Gaffney, I. R. Piletic, and M. D. Fayer, J. Chem. Phys. **118**, 2270 (2003).
[32] I. R. Piletic, K. J. Gaffney, and M. D. Fayer, J. Chem. Phys. **119**, 423 (2003).
[33] H.-S. Tan, I. R. Piletic, and M. D. Fayer, J. Chem. Phys. **122**, 174501 (2005).
[34] H.-S. Tan, I. R. Piletic, R. E. Riter, N. E. Levinger, and M. D. Fayer, Phys. Rev. Lett. **94**, 057405 (2004).
[35] I. Piletic, H.-S. Tan, and M. D. Fayer, J. Phys. Chem. B **109**, 21273 (2005).
[36] I. Piletic, D. E. Moilanen, D. B. Spry, and M. D. Fayer, J. Phys. Chem. A **110**, 4985 (2006).
[37] D. Cringus, J. Lindner, M. T. W. Milder, M. S. Pshenichnikov, P. Vohringer, and D. A. Wiersma, Chem. Phys. Lett. **408**, 162 (2005).
[38] A. M. Dokter, S. Woutersen, and H. J. Bakker, Phys. Rev. Lett. **94**, 178301 (2005).
[39] Q. Zhong, D. A. Steinhurst, E. E. Carpenter, and J. C. Owrutsky, Langmuir **18**, 7401 (2002).
[40] Q. Zhong, A. P. Baronavski, and J. C. Owrutsky, J. Chem. Phys. **118**, 7074 (2003).
[41] Q. Zhong, A. P. Baronavski, and J. C. Owrutsky, J. Chem. Phys. **119**, 9171 (2003).
[42] S. Woutersen, Y. Mu, G. Stock, and P. Hamm, Chem. Phys. **266**, 137 (2001).
[43] Y. S. Kim and R. M. Hochstrasser, Proc. Natl. Acad. Sci. U.S.A. **102**, 11185 (2005).
[44] E. L. Hahn, Phys. Rev. **80**, 580 (1950).
[45] I. D. Abella, N. A. Kurnit, and S. R. Hartmann, Phys. Rev. **14**, 391 (1966).
[46] C. P. Lawrence and J. L. Skinner, J. Chem. Phys. **117**, 8847 (2002).
[47] A. Piryatinski and J. L. Skinner, J. Phys. Chem. B **106**, 8055 (2002).
[48] C. P. Lawrence and J. L. Skinner, J. Chem. Phys. **118**, 264 (2003).
[49] C. P. Lawrence and J. L. Skinner, Chem. Phys. Lett. **369**, 472 (2003).
[50] A. Piryatinski, C. P. Lawrence, and J. L. Skinner, J. Chem. Phys. **118**, 9664 (2003).
[51] A. Piryatinski, C. P. Lawrence, and J. L. Skinner, J. Chem. Phys. **118**, 9672 (2003).
[52] S. Corcelli, C. P. Lawrence, and J. L. Skinner, J. Chem. Phys. **120**, 8107 (2004).
[53] J. R. Schmidt, S. A. Corcelli, and J. L. Skinner, J. Chem. Phys. **123**, 044513 (2005).
[54] R. Rey and J. T. Hynes, J. Chem. Phys. **104**, 2356 (1996).
[55] R. Rey, K. B. Møller, and J. T. Hynes, J. Phys. Chem. A **106**, 11993 (2002).
[56] K. B. Møller, R. Rey, and J. T. Hynes, J. Phys. Chem. A **108**, 1275 (2004).
[57] R. Rey, K. B. Moller, and J. T. Hynes, Chem. Rev. (Washington, D.C.) **104**, 1915 (2004).
[58] D. Laage and J. T. Hynes, Science **311**, 832 (2006).
[59] K. Kwac, H. Lee, and M. Cho, J. Chem. Phys. **120**, 1477 (2004).
[60] K. Kwac and M. Cho, J. Chem. Phys. **119**, 2256 (2003).
[61] K. Kwac and M. Cho, J. Chem. Phys. **119**, 2247 (2003).
[62] K. Kwac and M. Cho, J. Raman Spectrosc. **36**, 326 (2005).
[63] S. Kristyan and P. Pulay, Chem. Phys. Lett. **229**, 175 (1994).
[64] M. O. Sinnokrot, E. F. Valeev, and C. D. Sherrill, J. Am. Chem. Soc. **124**, 10887 (2002).
[65] S. Tsuzuki, K. Honda, T. Uchimaru, M. Mikami, and K. Tanabe, J. Am. Chem. Soc. **124**, 104 (2002).
[66] J. Cerny and P. Hobza, Phys. Chem. Chem. Phys. **7**, 1624 (2005).
[67] S. Tsuzuki and H. P. Luthi, J. Chem. Phys. **114**, 3949 (2001).
[68] C. Møller and M. S. Plesset, Phys. Rev. **46**, 618 (1934).
[69] K. Raghavachari, G. W. Trucks, J. A. Pople, and M. Head-Gordon, Chem. Phys. Lett. **157**, 479 (1989).
[70] Y. Jung, R. C. Lochan, T. Dutoi, and M. Head-Gordon, J. Chem. Phys. **121**, 9793 (2004).
[71] M. Feyereisen, G. Fitzgerald, and A. Komornicki, Chem. Phys. Lett. **208**, 359 (1993).
[72] S. F. Boys and F. Bernardi, Mol. Phys. **19**, 553 (1970).
[73] T. Helgaker, W. Klopper, H. Koch, and J. Noga, J. Chem. Phys. **106**, 9639 (1997).
[74] M. J. Frisch, G. W. Trucks, H. B. Schlegel *et al.*, GAUSSIAN03, Gaussian, Inc., Pittsburgh, PA, 2003.
[75] Y. Shao, L. F. Molnar, Y. Jung *et al.*, Phys. Chem. Chem. Phys. **8**, 3172 (2006).

[76] Y. Jung and M. Head-Gordon, Phys. Chem. Chem. Phys. **8**, 2831 (2006).
[77] P. F. B. Goncalves and H. Stassen, J. Chem. Phys. **123**, 214109 (2005).
[78] D. A. Case, D. A. Pearlman, J. W. Caldwell *et al.*, AMBER 8, University of California, San Francisco, 2004).
[79] E. M. Duffy, D. L. Severance, and W. L. Jorgensen, J. Am. Chem. Soc. **114**, 7535 (1992).
[80] T. Darden, D. York, and L. Pedersen, J. Chem. Phys. **98**, 10089 (1993).
[81] H. J. C. Berendsen, J. P. M. Postma, W. F. v. Gunsteren, A. DiNola, and J. R. Haak, J. Chem. Phys. **81**, 3684 (1984).
[82] J. R. Schmidt, S. A. Corcelli, and J. L. Skinner, J. Chem. Phys. **121**, 8887 (2004).
[83] S. Mukamel, *Principles of Nonlinear Optical Spectroscopy* (Oxford University Press, Oxford, 1995).
[84] M. Cho, J. Chem. Phys. **115**, 4424 (2001).
[85] M. F. DeCamp, L. DeFlores, J. M. McCracken, A. Tokmakoff, K. Kwac, and M. Cho, J. Phys. Chem. B **109**, 11016 (2005).
[86] O. Golonzka and A. Tokmakoff, J. Phys. Chem. B **115**, 297 (2001).
[87] S. Park, K. Kwak, and M. D. Fayer (unpublished).
[88] A. P. Scott and L. Radom, J. Phys. Chem. **100**, 16502 (1996).